Journal of Biological Methods | **2021** | **Vol**. 8(1) | e142
DOI: 10.14440/jbm.2021.348

ARTICLE

Visualization of subdiffusive sites in a live single cell

Zeno Földes-Papp[1‡*], Gerd Baumann[2], Long-Cheng Li[3]

[1]Head of the Department of Geriatrics, Asklepios Clinic Lindau, 88131 Lindau (at Lake Constance), Bavaria, Germany
[2]Head of the Mathematics Department, Faculty of Basic Sciences, German University in Cairo (GUC), 11835 New Cairo City, Egypt
[3]Institute of Reproductive Medicine, School of Medicine, Nantong University, Nantong 226001, China

*Corresponding author: Zeno Földes-Papp, Email: zeno.foldespapp@gmail.com

‡Zeno Földes-Papp holds the permanent position of a Visiting Professor at the Mathematics Department and Faculty of the GUC, in memoriam RFP.

Competing interests: The authors have declared that no competing interests exist.

Abbreviations used: Ago2, argonaute 2; EGFP, enhanced green fluorescence protein; FCS, fluorescence correlation spectroscopy; LNA, locked nucleic acid; LSM, laser scanning microscopy; PCH, photon counting histogram; PC-3, prostate cancer cells; RICS, raster image correlation spectroscopy; SIM, structured illumination microscopy; SQ, superquencher; SQMB, superquencher molecular beacon; STED, stimulated emission depletion; TIRF, total internal reflectance fluorescence

Received October 25, 2020; Revision received December 5, 2020; Accepted December 5, 2020; Published January 30, 2021

ABSTRACT

We measured anomalous diffusion in human prostate cancer cells which were transfected with the Alexa633 fluorescent RNA probe and co-transfected with enhanced green fluorescent protein-labeled argonaute2 protein by laser scanning microscopy. The image analysis arose from diffusion based on a "two-level system". A trap was an interaction site where the diffusive motion was slowed down. Anomalous subdiffusive spreading occurred at cellular traps. The cellular traps were not immobile. We showed how the novel analysis method of imaging data resulted in new information about the number of traps in the crowded and heterogeneous environment of a single human prostate cancer cell. The imaging data were consistent with and explained by our modern ideas of anomalous diffusion of mixed origins in live cells. Our original research presented in this study is significant as we obtained a complex diffusion mechanism in live single cells.

Keywords: anomalous diffusion, complex diffusion mechanism, imaging, live cell, number of traps

INTRODUCTION

Diffusion dynamics has been the constant topics in recent years in literature, especially, in single-molecule literature on solid phase and imaging. The merging of biology and imaging to explore biological processes at the level of single cells facilitates the identification of genetic modifiers as well as monitoring of the drug response in live cells [1]. Fluorescence microscopy has become a fundamental technique in life science research. It is a selective technique, as it enables the isolation and examination of individual biological features which have been labeled with a fluorescent dye, also known as a marker. The use of a marker allows the area bound to the dye to become illuminated under the microscope, leaving other regions dark, which enables a specific region to be examined. When a higher spatial resolution is required total internal reflectance fluorescence (TIRF) microscopy techniques and super-resolution techniques, such as structured illumination microscopy (SIM) and stimulated emission depletion (STED) microscopy, are the methods of choice [2].

In confocal techniques like fluorescence correlation spectroscopy (FCS), laser scanning microscopy (LSM) and photon counting LSM (there are very few of them around) the same measured fluorescence intensity fluctuations are used [3]. However, each analytical technique focuses on a different property of the signal. The time-dependent decay of the correlation of fluorescence fluctuations is measured in FCS yielding, for example, the molecular diffusion coefficients and its correlation amplitude yielding the numbers of diffusing molecules. The amplitude distribution of these fluctuations is calculated by photon counting histogram (PCH) yielding the molecular brightness. Actually the counterparts of FCS and PCH are raster image correlation spectroscopy (RICS) and number and brightness analysis, respectively. Confocal LSM works on the principle of point excitation in the specimen (diffraction limited spot) and point detection of the resulting fluorescent signal (fluorescence intensities). It allows for labeled molecules to be accurately pinpointed within the cell.

Here, we tested our modern ideas of anomalous diffusion in human prostate cancer cells. The detection system consisted of the argonaute2 (Ago2) fused to enhanced green fluorescence protein (EGFP) referred to EGFP-Ago2 and the dark target Alexa633-SQ-dsP21-322 RNA molecules where the fluorescent dye Alexa633 is quenched by its so-called superquencher (SQ) [4]. When the EGFP-Ago2 fusion was coexpressed with the target RNA in a human prostate cancer cell, a large number of tagged proteins EGFP-Ago2 bound to the antisense

How to cite this article: Földes-Papp Z, Baumann G, Li LC . Visualization of subdiffusive sites in a live single cell. *J Biol Methods* 2021;8(1):e142. DOI: 10.14440/jbm.2021.348

strands of Alexa633-SQ-dsP21-322 RNA formed bright fluorescent particles with an estimated physical size in the order of about 100 nm. The fluorescent molecules EGFP-Ago2 and their RNA complexes can be followed under microscope since the labeled RNA contained nuclease protected LNA nucleotides which were much longer lived than endogenous RNA allowing us to follow them for many minutes. The tagged RNA and the EGFP-Ago2 molecules moved randomly in the cell compartments (cytoplasm, nucleus or membranes) spanning the complete compartment length. The image data of the human prostate cancer cells were acquired by confocal LSM simultaneously at 633 nm excitation for the Alexa633 RNA probe and 488 nm excitation for the EGFP-Ago2 in co-localization experiments. The results obtained were consistent with and explained by our modern ideas of anomalous diffusion. The concept assumed that traps were not immobile and extracted their number from confocal LSM image series in live cells. The anomalous translational subdiffusion describes spatial and heterogeneous (temporal) randomness in cellular systems as it was proposed in the study by Földes-Papp *et al*. [5]. A similar biological interpretation was proposed independently by Gratton and colleagues [6,7].

METHODS AND MATERIALS

Formulation of the problem

Single-molecule level

The issue with stochastic thermodynamics is a very high level of abstractness of the probabilistic equations in order to describe the stochastic nature of translational diffusion [8,9]. Stochastic thermodynamics rules the physical formulation of the single-molecule time-resolution T_m. Let us denote by the equation (1) T_m with respect to the measurement of the same molecule in dilute liquids and live cells without immobilization or significant hydrodynamic flow

$$T_m = \tau_{dif} \cdot K \qquad \text{Eqn. (1)}$$

where K stands for the proportionality factor and it was specified by

$$K = \frac{e^{(c_m \cdot N_A \cdot \Delta V)}}{c_m \cdot N_A \cdot \Delta V} \qquad \text{Eqn. (2)}$$

K was essentially related to the number of molecules in the observation volume ΔV and it is constant for the experimental setup (thermodynamic setup) $K_{|c_m, \Delta V = const.} = const.$.

e^N is the natural exponential function of the number of molecules N in the observation volume ΔV and N is determined by the product $c_m \cdot N_A \cdot \Delta V$ with $N < 1$,

c_m is the molar concentration of molecules of the same kind in the bulk (bulk phase),

N_A is the Avogadro constant (number) and it is defined as $N_A = 6.02214076 \times 10^{23}$ mol^{-1},

τ_{dif} is the diffusion time of the same single molecule (selfsame and individual molecule, respectively) and

T_m is the meaningful time of measuring one and the same molecule in dilute liquids and live cells without immobilization or significant hydrodynamic flow, which is the single-molecule time-resolution in microscopy, nanoscopy and spectroscopy. It is a natural law.

Obviously, the dimension of T_m is the dimension of τ_{dif}.

Why are the above equations (1) and (2) so attractive? There is direct and simple connection with measurements. This connection is based on the diffusion times of molecules. In fact, all conditions are only properties of the stochastic nature of diffusion times of single molecules. In the original papers published in 2006 and 2007 [8,9], where the equations (1) and (2) and the concentration dependence of this modern theory of single-molecule detection at the level of the individual molecule, *i.e.*, one and the same molecule, was formulated for the very first time, the derivations of the equations, remarks and explanations were given to justify the experimental conditions (criteria 1 to 3, the equations (1) and (2) are the criterion 4). In this theory, diffusion times are directly linked to selfsame molecule likelihood estimators as a consequence of the stochastic analysis of the thermodynamic system considered. Further, why is the proportionality factor K of the equation (1) specified by the equation (2)? This is only because of the stochastic nature of diffusion. Of course, these conditions are only technical conditions, which however must be fulfilled in order to apply the equations (1) and (2) to measurements. Thus, the language of stochastic thermodynamics [8,9] is the main advantage of the theory of single-molecule detection at the level of the individual molecule.

Is it possible to generalize the equation (1)? Yes, it is possible and for the very first time it was done in the original article [10] by the equation (3)

$$T_m(t) = \tau_{dif}(t) \cdot K \qquad \text{Eqn. (3)}$$

where t is the time, for example the measurement time. The equation (3) would be attractive by the same reasons as the equations (1) and (2). Moreover, the meaningful times T_m and $T_m(t)$ refer to the precision of a measurement in microscopy, nanoscopy (super-resolution microscopy) and spectroscopy with respect to the time of measuring just one and the same molecule in dilute liquids and live cells without immobilization or significant hydrodynamic flow that was first proved by the equations (1) and (2) in the study by Földes-Papp [9]. Thus, the single-molecule time-resolution T_m and $T_m(t)$ are the counterpart of the space-resolution in optical microscopy imposed by the wave nature of light and first established by Ernst Abbe's well-known formula in 1873 (Abbe refers to a self-emitter) and later refined by Lord Rayleigh in 1896 (Rayleigh refers to a fluorescent emitter) to quantitate the measure of separation necessary between two Airy patterns in order to distinguish them as separate entities.

First, let us recall some of the main ideas of the equation (1) and its concentration dependency emerged in a paper that was published in 2004 and 2005, respectively [11]. The theory is mainly based on two facts: (i) the existence of a continuity equation and (ii) the existence of a probability current. This new development may lead to a clarification of concepts used in widely different fields of medical genomics and proteomics such as biochemistry, molecular biology, and immunology. In all these fields, we find again and again the same questions: what is the meaning of single-molecule approaches? Are they just another tool? Can we be sure of measuring just one molecule, *i.e.*, the self-same molecule? What is the impact of measuring the single molecule that means the self-same molecule?

Here, we are mainly interested in some properties of the generalized equation (3). The first one is the time-dependency of the diffusion time. This principle is well-known in physics as anomalous diffusion.

Anomalous diffusion is a diffusive process with a non-linear relationship between the mean squared displacement and time. We only consider subdiffusion. Physically, the space that the molecules explore refers to a scaling exponent with values smaller than 1. The second property of the generalized equation (3) is the principle of randomness. According to this principle the challenge is to understand the underlying mechanism which causes it.

Taken together, the basic relationships are summarized in equations, for example in the equations (1) to (3). The deductive reasoning does not require any data. This is the effectiveness of the formulas with which we precisely describe the real conditions, some of which are far beyond what can be observed with current technologies [10,12,13]. In other words, the theory and its natural laws (see equations (1), (2) and (3)) have practical uses and consequences. Hence, we considered here the many-molecule level.

Many-molecule level

At the many-molecule level we did not consider here pair correlations between different positions of molecules [7], although the attractive approach provided more parameters such as the path followed by molecules. Instead, we analyzed the wide-view imaging at diffraction-limited spatial resolution and obtained a complex diffusion mechanism (see RESULTS AND DISCUSSION). A universal biological principle described the cellular function from the combined interactions of molecules and sub-cellular structures in time and space. Interactions typically revealed themselves through statistical dependencies in the spatial distribution of the involved molecules and sub-cellular structures at the many-molecule level [14]. We used this general explanation, and we therefore explained interactions as the set of all effects that cause correlations in the positions of the participating molecules in time and space. This is where the pair correlation approach could also be applied.

Organelle shape considerably influences diffusive motion and therefore transport and must be taken into account when relating experimental data to diffusion times. Trapping molecules in live cells can exert at least two types of effects that could be important for function. First, live cells will have a strong influence on how far and how fast locally produced molecules will travel within the cytoplasm, the nucleoplasm or the membranes. Over a time scale of 1 s, a molecule with an apparent diffusion coefficient D_{app} of 2 µm²/ms, would diffuse about 60 µm. Thus, as long as molecules remain within the cytoplasm, nucleoplasm or the membranes, their movement could be dominated by an anomalous diffusion process over distances. Second, anomalous diffusion reflects an increase in the spatial and temporal heterogeneity of diffusing molecules which would be expected to promote activation of biochemical networks by intracellular signals trapped in live cells. The concept of barrier to motion is detailed in the next paragraph.

In a crowded environment like a cell or its nucleus, the cytoplasm, or the nucleoplasm are made up of different steric obstacles like vacules or membranes by which the diffusive motion of molecules is slowed down. These steric hindrances are structure-dependent traps. Beside the steric traps, there are single strongest binding sites that are the target sites of molecules. It is reasonable that there may be many weak binding sites, which correspond to nonspecific binding sites. There may be a number of intermediate binding sites where weak binding depends on how similar they are to the target site. The simplest way to conceive a hierarchy of interaction sites is to distinguish between structure-dependent (space heterogeneity) and rate-dependent (temporal heterogeneity) traps. The labeled molecules move randomly in the cell compartment spanning the complete compartment length. Once in a "great while", the diffusing molecules will be delayed in the dangling ends, bottlenecks and backbends existing in the cell or/and by reacting with a binding site (reaction partner). In both cases, the labeled molecule is "trapped" in one location. The trapping has either a steric origin or a temporal origin with the molecule binding to interaction sites which means it is of mixed origins.

Model of numbers of traps in crowded and heterogeneous environment of living cells and their compartments at the many-molecule level

The main purpose of this subsection is to describe the theoretical model arising from "two-level systems" and to show how analysis of experimental data with this model lead to information about the number of traps at which the diffusive motion is slowed down in crowded and heterogeneous environment. It is thought that the types of motions result from the flipping (fluorescence signal fluctuation) of two-level systems. The level X represents the situation where the molecules are inside the femtoliter-sized observation volume ΔV and fluorescence is detected. The level Y is assigned if the molecules diffuse out of ΔV and no fluorescence is detected. The labeled molecules proceed through substates $X_2, X_3, ..., X_v$, for example different local environments. Thereby, they undergo $v-1$ traps from state X_1 inside ΔV to state Y_1 outside ΔV with rate β. A similar series of steps is required for the reverse process from state Y_1 outside ΔV to state X_1 inside ΔV. In principle, the value of v for diffusive motion out of ΔV could be different from that for the diffusive motion into ΔV. Here, we consider the case where they are the same. The scheme of interactions originating from randomness (heterogeneity) by traps is given in the relationship (4)

$$\begin{pmatrix} X_1 & \xrightarrow{\beta} & X_2 & \xrightarrow{\beta} & \dots & \xrightarrow{\beta} & X_v \\ \beta\uparrow & & & & & & \beta\downarrow \\ Y_v & \xleftarrow{\beta} & \dots & \xleftarrow{\beta} & Y_2 & \xleftarrow{\beta} & Y_1 \end{pmatrix} \quad \text{Eqn. (4)}$$

Relationship (4) looks like a matrix but it is not. The relationship (4) shows that there are $v-1$ different events and traps, respectively. A series of first-order events, each event occurring at rate β, is necessary for switches $Y \rightarrow X$ and $X \rightarrow Y$ to happen. The stochastic switching between inside and outside ΔV is of variable duration. The amount of time spent in state X ("on" times) or Y ("off" times or times between fluctuation maxima) can be well described by a gamma distribution, which has the probability density

$$p_t(\Delta t) = \frac{\beta^v \cdot \Delta t^{v-1} \cdot exp\{-\beta \cdot \Delta t\}}{\Gamma(v)} \quad \text{Eqn. (5)}$$

with parameters v and β. $\Gamma(v)$ is the gamma function. The equation (5) is the convolution of exponential distributions. The parameter $v-1$ is consistent with the number of traps. Equation (5) is essentially what we used to calculate the number of traps from the experimental image data (see Image processing by the TZ Fluctuation Analyzer software version 1.2.2). Equation (5) is not derived or extended from the equation (1) and (2).

We adopted equation (5) from literature [15] and we also under-

stood interaction as the collection of all effects in the positions of the participating molecules [16]. Evidence has been accumulated for anomalous subdiffusive motion of molecules in various eukaryotic systems [16]. To avoid any confusion, here we defined a trap as any subdiffusive site in the cell and analyzed the number of traps $v-1$ in the single live cell. In other words, we used the term trap to mean that at this spatial position the diffusion is slowed down by a subdiffusive site compared to normal diffusion. If there is no trap, *i.e.*, $v = 1$, we obtain the scalar function $\eta(t)$ of binary states $1 = X_1$ inside ΔV and $0 = Y_1$ outside ΔV for normal diffusive motion [17]. For normal diffusive motion of fluorescent molecules with no traps, we previously showed that the probability density of times between fluctuation maxima is negative exponential [17]

$$p_t(\Delta t) = \beta \cdot \exp\{-\beta \cdot \Delta t\} \qquad \text{Eqn. (6)}$$

and the times between fluctuation maxima are broadly distributed. If v is large, the gamma distribution in equation (5) is symmetric and narrowly distributed about the mean v/β. At the other extreme, if $v \to \infty$ then all times between fluctuation maxima are equal.

The equations (4) and (5) relied on experimental observations that generate a signal upon the proximity required for molecular interaction. This allowed us to study sets of sequences of events in images. From the measured probability density of times between fluctuation maxima in fluorescence intensity time traces, we obtained the number of traps $v-1$ (see Results and Discussion).

Experimental design of the test system

Double-stranded small RNAs (dsRNAs) that are complementary to non-coding transcripts at gene promoters can activate or inhibit gene expression in mammalian cells. The argonaute protein Ago2 is recruited to the non-coding transcript that overlaps the promoter during both gene silencing and activation [18,19,20]. p21 was susceptible to RNA activation by dsP21-322 RNA in prostate adenocarcinoma cells (PC-3) [18,21,22].

As shown in **Figure 1**, we chemically synthesized the SQ-probes with nuclease protection by LNA nucleotides (for LNA in imaging, see [23]). LNA nucleotides were used as the antisense and the sense strand of the dsRNA-duplex. We applied the red fluorescent dye Alexa Fluor 633 absorbing at 633 nm and emitting at 650 nm. After binding to Ago2, the SQ-probe directed against the antisense strand will remain a dark probe, whereas the respective guide strand lightens up and can be measured by confocal laser scanning microscopy in the crowded environment of the cytoplasm and/or the cell nucleus. We previously showed that p21 was susceptible to RNA activation by specific binding of dsP21-322 RNA to Ago2 by forming a complex in a variety of cells lines including PC-3 cells (see ref. [22] and the articles cited therein). Ago2 could be found in both nuclear and cytoplasmic compartments of the cells [22,21]. Molecular beacons that included energy transfer pairs of Alexa Fluor 633 and SQ as dark acceptor (that is the molecule named BHQ3) were used before for direct probing of unamplified genomic DNA by homogeneous hybridization using two-color fluorescence cross-correlation technique [24,25] and for detecting microRNA122 in live cells [23].

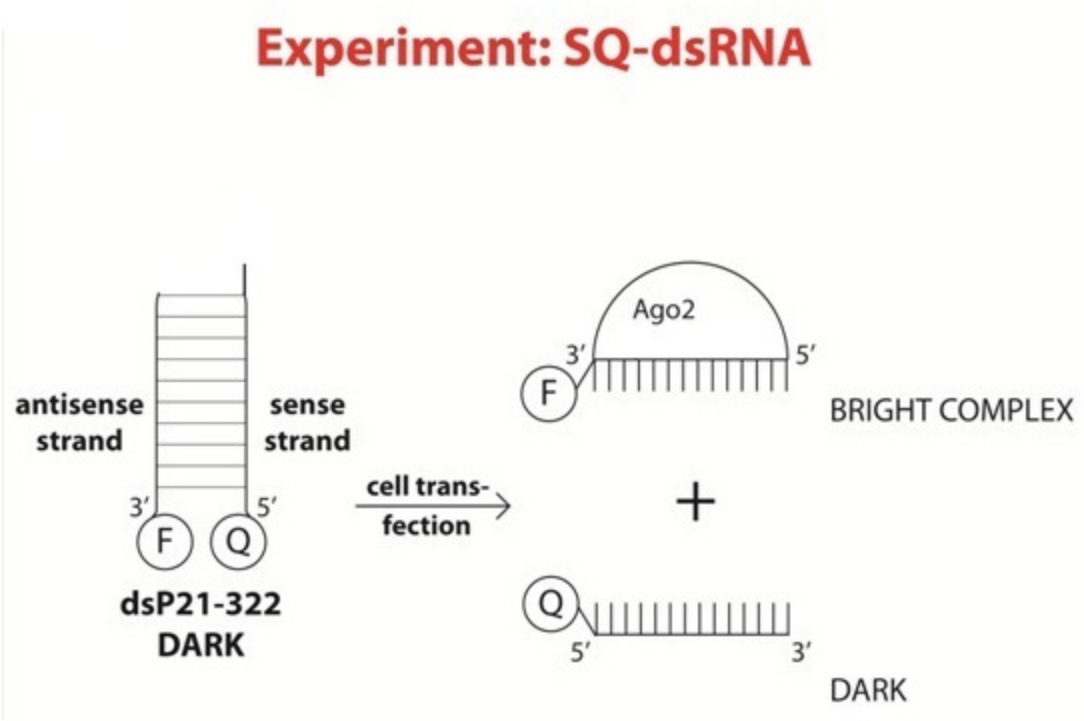

Figure 1. Schematic depiction of the experiments with dsP21-322 RNA. We used so-called superquencher dsRNA duplexes (SQ-dsRNA), which were dark probes in unbound state. F stands for the fluorophore Alexa633 and Q for the superquencher BHQ3 which is not fluorescent. In the co-localization experiments with EGFP, we co-transfected end expressed EGFP-Ago2 in the humanPC3.

Cell culture and transfection experiments

Human PC-3 were transfected with Alexa633-SQ-dsP21-322 RNA. The cells were co-transfected with fusions of EGFP and Ago2. Cells were grown and treated as described previously and all experimental conditions were given in details in [22].

Confocal laser scanning microscopy

ZEISS confocal laser-scanning microscope LSM510 META [3,26] was used for the scanning measurements. The microscope came with four confocal channels for reflected light, plus one for transmitted light. Each channel had individual 12-bit analog-to-digital converters to ensure optimum data acquisition. The LSM 510 used Digital Signal Processor to control data acquisition, scanner operation, and the acusto-optical tunable filters (AOTFs) and it had the capability to change the settings for lasers and detectors very quickly. AOTF was used for tuning the power of each laser line and image acquisition, which means multiple regions of any shape were selected, scanned with specified laser power, and detected with optimized settings. Another unique feature was the META spectral detection system, which gave the emission spectra at each pixel. This spectral signature facilitated the deconvolution of overlapping dyes and probes. Specialized software for 3D image processing was available for image analysis, including automated measuring functions for the quantitative analysis of 3D and 4D (*i.e.*, time) data sets.

In the fluorescence imaging experiments, the single living cell was scanned with the excitation laser beam and, thus, not only the fluorescence coming from one excitation volume but from a larger area was detected without loss of spatial resolution. We started with the database 121610-5.mdb. The optical section z_1 showing a section through the cytoplasm and the nucleus of human PC-3 gave very bright fluorescence of the fluorescent probes. The z-value was sampled with about 400 time points in both detection channels. One detection channel was for the red emission of the Alexa633 fluorescent probe and the second detection channel was for the green emission of the EGFP-Ago2. The image data were acquired simultaneously at 633 nm excitation for the Alexa633 probe and at 488 nm excitation for the EGFP-Ago2. All parameter settings were optimized.

The database 121610-4.mdb contained the files mocklowintensity.lsm, which were the autofluorescence background of the human PC-3 at the red excitation of 633 nm and at the blue excitation of 488 nm for the same laser power and z positions as in the database 121610-5.mdb. This gave good background values of autofluorescence and crosstalk between the two detection channels which were subtracted from the image files with fluorescent probes (121610-5.mdb).

Of course, the instruments have gotten better, for example in the LSM710 and the LSM780 we sampled in the pixel with 40 MHz. In the LSM510 META we still had a capacity charged so that ca. 30% of the signal was lost during the discharging process and the duty cycle was therefore lower. Nevertheless, reference [27] demonstrated that the LSM510 META was suitable for fluctuation analysis and provided useful and reliable results. Using other instruments no essentially different results come out.

The pixel resolution depended on the lens NA and was calculated using Rayleigh's formula. For example, we measured 500 nm with the 40×1,2 ZEISS objective, then according to Rayleigh the spatial resolution was approximately 245 nm. We then scanned with a step size of 124 nm to get this spatial resolution. But actually it was not that important; if we typically chose a pixel size of 1 µm, our spatial resolution was half that value.

Image processing by the TZ Fluctuation Analyzer software version 1.2.2

The collected fluorescence photon stream data were analyzed by the procedures of the Fluctuation Analyzer TZ [28]. We searched for the peak-like characteristics in the data, where photon counts increased and then decreased. If the photon counts at the local maximum were above a certain threshold level, the software considered it as a fluctuation and saved the time position and photon counts of the local maximum at its spatial position. The Fluctuation Analyzer also saved the time position of the start and the end of each peak shape.

Fluorescent intensity fluctuations in the diffusion-based detection scheme of time series were identified by this analysis procedure with respect to their intensity and location and fitted to the equation (5). The χ^2-criterion was used for linking the experimental data of time series at each spatial position (pixel) of the laser scans to the equation (5). The best fit values for the number of traps $\nu-1$ were plotted across the spatial positions (pixels) in the scans as shown in **Figure 2B** and **2D**.

RESULTS AND DISCUSSION

In a typical experiment, a sample was taken from a growing culture of cells containing a low level of target RNA as well as saturating numbers of EGFP-Ago2 tagging proteins. Cells were imaged with ZEISS Confocal Laser-Scanning Microscope LSM510 META. Cells were tracked for up to 30 min at 1 frame/s.

A single human prostate cancer cell with its cytoplasm and nucleus is shown in **Figure 2**. The horizontal and vertical axes corresponded to the x and y coordinates in pixel lengths. In **Figure 2A** and **2C**, an optical section z_1 through a single cell is shown. The red detection channel in **Figure 2A** was for the red emission of the Alexa633 fluorescent probe SQ-dsP21-322. The green detection channel in **Figure 2C** was for the green emission of the co-transfected and expressed EGFP-Ago2. The image data were acquired simultaneously at 633 nm excitation for the Alexa633 probe (**Fig. 2A**) and 488 nm excitation for EGFP-Ago2 (**Fig. 2C**). The z_1-value was sampled with about 400 images at different time points in both detection channels and the background (autofluorescence and crosstalk between the two detection channels) were subtracted from the cell images. The data of **Figure 2** were obtained over the measurement time of about 30 min.

The measured counts were color-coded for the red emission (**Fig. 2A**) and the green emission (**Fig. 2C**). In the image series of the labeled Alexa633 fluorescent probe SQ-dsP21-322 molecules (B) and the EGFP-Ago2 labeled molecules (**Fig. 2D**), we extracted the number of traps at the same optical section z_1 by means of the equation (5). The numbers of traps $\nu-1$ were also color-coded for the red emission (**Fig. 2B**) and the green emission (**Fig. 2D**). We found that the number of traps $\nu-1$ was in the range of about 2−3 to 7−8. The analysis demonstrated that they are quite similar in cytoplasm and nucleus as well as membranes. The imaging data obtained were consistent with and explained by anomalous-subdiffusive sites, which were distributed all over the cell.

dsRNA duplex (SQ-dsRNA) were dark probes in unbound state but lightened up to maximum fluorescence after binding to their target. We should expect to see only two dots or a focused signal in the nucleus since

the target of the dsRNA was at the promoter of the gene p21, although the dsRNA could bind to sites with partial homology. In **Figure 2B** and **2D**, the signal was quite disseminated. Because our approach was at diffraction-limited optical resolution, so it was more suitable for measuring global anomalous subdiffusion than for resolving single events (interactions).

The method (relations (4) and (5)) is a convolution of exponential functions in form of the gamma distribution density. The method assumes that traps are not immobile and extracts their numbers in crowded and heterogeneous environment of living cells as visualized in **Figure 2B** and **2D**. The method is based on diffusion arising from the "two-level systems": A trap is a site in the living cell where the diffusive motion is slowed down. Once in a while, tagged RNA molecules will react with the reaction partner EGFP-Ago2 (see **Fig. 1**). Thus, the tagged RNA molecules become visible and are "trapped" in one location. The formed complexes between labeled RNA-Ago2 and their target are also spreading by diffusion. The trapping has a temporal origin with the molecule binding to interaction sites. Indeed, these interactions make a contribution to the fluorescence signals in addition to the motion of free EGFP-Ago2 molecules. Moreover, the argonaute2 protein complexes could search for higher-order structure in the DNA of the nucleus in order to activate p21 expression. Furthermore, it is reasonable that there are many weak binding sites, which correspond to nonspecific binding sites. It is well known that anomalous diffusion may result from obstruction [16]. Trapping mechanisms are changes in localization like entry of a DNA-binding regulatory protein into the nucleus or assembly of a functional enzymatic complex or conformational changes in the diffusing species or intracellular obstacles like organelles hindering diffusion. A simple way to conceive a hierarchy of interactions (and obstruction) sites is equation (5).

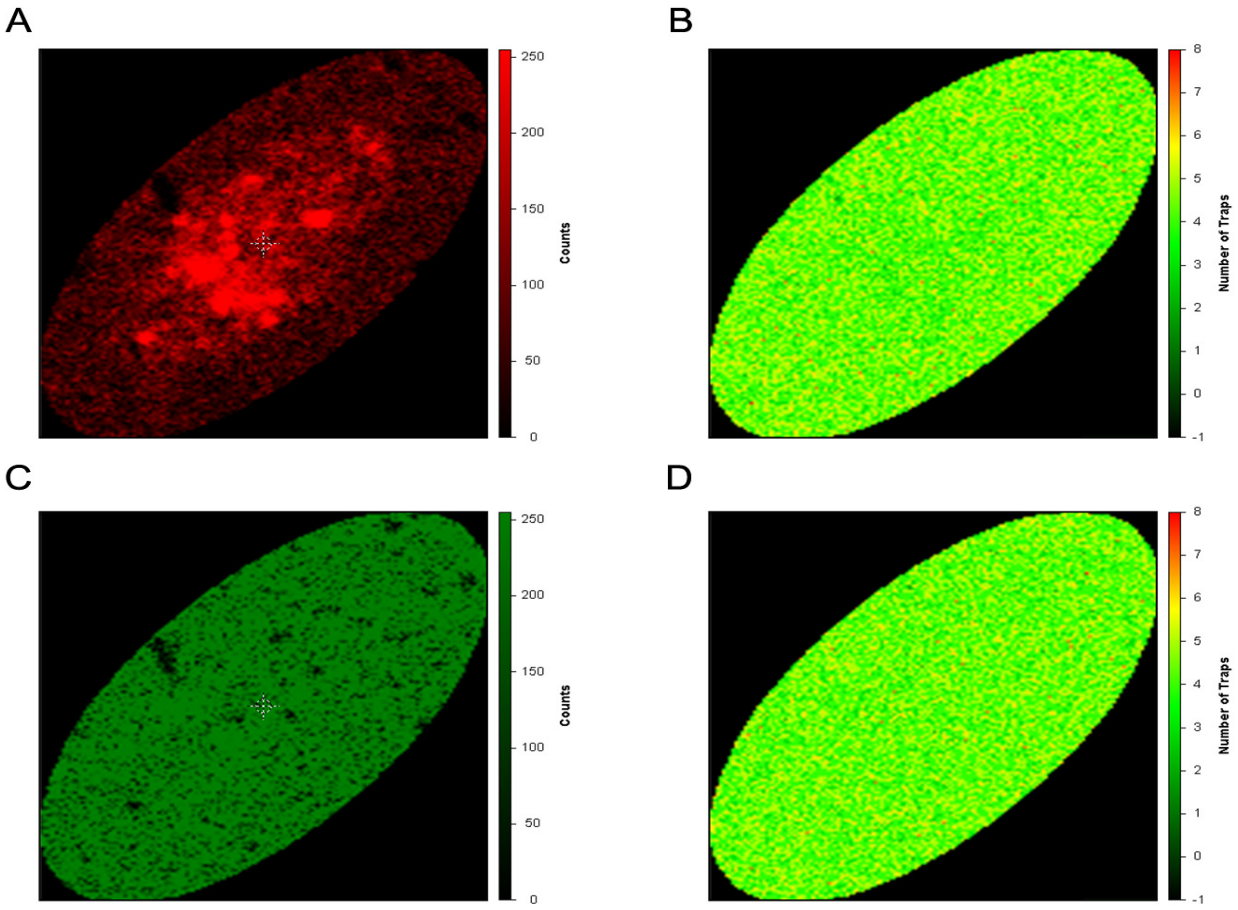

Figure 2. Human PC3 expressing EGFP-Ago2 and transfected with the Alexa633-tagged dsRNA probe were measured by confocal LSM. The horizontal and vertical axes corresponded to the x and y coordinates in pixel lengths. **A** and **C.** Confocal LSM images show the tagged RNA and EGFP-Ago2 molecules moving randomly in a whole single live cell. The measured counts were color-coded for the red emission (A) and the green emission (C). The images were taken at the z coordinate z_1. The depicted z_1- value was sampled with about 400 images at different time points in both detection channels. The background values of autofluorescence and crosstalk between the two detection channels were subtracted from the cell images (see Confocal laser scanning microscopy). The optical section z_1 in (A) and (C) gave very bright fluorescence. The image data were acquired simultaneously at 633 nm excitation for the Alexa633 probe and at 488nm excitation for EGFP-Ago2. The red detection channel (A) was for the emission of the Alexa633 labeled fluorescent probe SQ-dsP21-322 RNA. The green detection channel (C) was for the emission of the co-transfected and expressed EGFP-Ago2. **B** and **D.** Numbers of traps $v-1$ based on complex diffusion of the labeled molecules in the time-dependent image series taken at the same x and y coordinates of optical section z_1. The numbers of traps $v-1$ was calculated from the two-level systems by the equation (5). A trap was a site in the living cell where the diffusive motion was slowed down (see main text for explanations).

Our results confirm by a different measurement approach that subdiffusion seems to be a general phenomenon in biological cells. Gratton and colleagues used pair-correlations to detect diffusion barriers [6,7]. In spatial pair-correlation, diffusion is measured by the average time particles (molecules) take to travel between two points as the position of the two points is arbitrary. A laser beam is moved rapidly to different locations in a repeated pattern, *e.g.*, a line, circle, or grid. The entire pattern is repeated in approximately 1 to 10 ms. If there is a barrier to diffusion that may called trap, the particle goes around the obstacle or passes over the barrier (binding interaction). The maximum of the spatial pair-correlation function will be found at a longer time than in the absence of a barrier. By mapping the time of the maximum of the pair-correlation function, for every pair of points in the image, the location and the size of the obstacles can be visualized. By fitting the series of correlation functions, the actual protein "diffusion law" can be obtained directly from imaging, in the form of a mean-square displacement *vs*. time-delay plot. Lu and colleagues published work on analyzing multiple-step conformational state diffusion in multiple-state rate processes [29]. They usually have to analyze a large database on time-resolved diffusion trajectories to characterize the diffusion dynamics; and that is an advantage of our unique analysis that can reveal the information without diffusion trajectories. Our work presented in this study is significant as we obtain a complex diffusion mechanism. Jin Wang from SUNY Stony Brooke and Eli Barkai published some very significant works on non-poisson statistics in analyzing diffusion dynamics, not only the molecules diffusion in biological systems but also on the theory of classical systems in complex energy landscapes, such as the complex protein conformational dynamic diffusions and reaction rate fluctuation diffusions [30,31].

Why are these results, which were independently obtained by different measurement methods, important? They clearly show that regardless of the measurement method used, subdiffusion must be taken into account in biological cells and their compartments. Otherwise the fitting parameters, for example in fluorescence correlation spectroscopy methods or fluorescence photobleaching, are worthless, *i.e.*, they are incorrect because the underlying evaluation model does not correctly reflect the biological facts. That is the main result of our original paper (for separation of the spatial subdiffusion from the temporal subdiffusion in measurements see ref. [32]: pick up the dynamic information of molecules from a live cell).

CONCLUSIONS

The original paper described FCS studies on an Alexa633 labeled RNA probe and green fluorescent protein-labeled argonaute2 protein in human prostate cancer cells. An interesting and originally "twist" to the experiments was the use of a so-called superquencher, BHQ3, which is not fluorescent, but which quenches the Alexa633 labeled RNA when it is in the duplex form. When the RNA strands dissociate upon binding to the EGFP-argonaute2 protein the Alexa633 then fluoresces brightly.

We investigated human PC-3 cells expressing EGFP-Ago2 and transfected with the Alexa633-tagged dsRNA probe. Our mathematical approach, fully described in the text, was a convolution of exponential functions in form of the gamma distribution density. The method assumed that traps were not immobile and was able to extract their numbers in crowded and heterogeneous environment of living cells. Using our novel analysis method of imaging data allowed us to obtain new information about the number of traps in a crowded and heterogeneous cellular environment. The theory and experimental approach, using two different laser wavelengths, were described in sufficient detail to allow others to replicate their findings and apply to approach to other biological systems.

The work appears to be a highly original and significant addition to the growing armamentarium of FCS and LSM techniques. The research article is an interesting paper about a complex diffusion occurring in live cells. In a crowded cell environment one can expect such complexity.

Acknowledgments

The analysis was performed by means of the software package TZ Fluctuation Analyzer version 1.2.2, which was developed by Drs. Zeno Földes-Papp and Tiefeng You, who was the main software programmer at ISS Inc, Champaign, IL, USA. We also thank Dr. Tiefeng You for his comments on the manuscript. This study would not have been possible without the support of Dr. Beniamino Barbieri, who is the president of ISS, 1602 Newton Drive, Champaign, IL-61822, USA. The cell transfection experiments were performed in the laboratory of Dr. Long-Cheng Li at the Helen Diller Comprehensive Cancer Center, University of California, San Francisco, CA, USA by Drs. Vera Huang and Long-Cheng Li.

We would like to thank Drs. Julian Borejdo, professor, Dept. of Molecular Biology and Immunology, Graduate School of Biomedical Sciences, University of North Texas Health Science Center, Dallas-Fort Worth, TX, USA, Enrico Gratton, BME professor, University of California, Irvine, CA, USA, Ignacy Gryczynski, professor, Dept. of Molecular Biology and Immunology, Graduate School of Biomedical Sciences, University of North Texas Health Science Center, Dallas-Fort Worth, TX, USA, H. Peter Lu, professor of chemistry, Dept. of Chemistry, Center for Photochemical Sciences, Bowling Green State University, Bowling Green, OH, USA and Klaus Weisshart, ZEISS Research Microscopy Solutions (Confocal LSM), Headquarters, Jena, Germany, for the background reading of the manuscript and their helpful comments.

Zeno Földes-Papp would also like to thank Dr. David Jameson, professor, Dept. of Cell and Molecular Biology, University of Hawaii, Manoa, Honolulu, HI, USA for his continuous support of the research over the years.

References

1. Jonkman J, Brown CM, Wright GD, Anderson KI, North AJ (2020) Tutorial: guidance for quantitative confocal microscopy. Nat Protoc 15: 1585-1611. doi: 10.1038/s41596-020-0313-9. PMID: 32235926
2. Ward EN, Pal R (2017) Image scanning microscopy: an overview. J Microsc 266: 221-228. doi: 10.1111/jmi.12534. PMID: 28248424
3. Weisshart K, Jüngel V, Briddon SJ (2004) The LSM 510 META - ConfoCor 2 system: an integrated imaging and spectroscopic platform for single-molecule detection. Curr Pharm Biotechnol 5: 135-154. doi: 10.2174/1389201043376913. PMID: 15078148
4. Yang CJ, Lin H, Tan W (2005) Molecular assembly of superquenchers in signaling molecular interactions. J Am Chem Soc 127: 12772-12773. doi: 10.1021/ja053482t. PMID: 16159250
5. Földes-Papp Z, Baumann G (2011) Fluorescence molecule counting for single-molecule studies in crowded environment of living cells without and with broken ergodicity. Curr Pharm Biotechnol 12: 824-833. doi: 10.2174/138920111795470949. PMID: 21446904

6. Digman MA, Gratton E (2011) Lessons in fluctuation correlation spectroscopy. Annu Rev Phys Chem 62: 645-668. doi: 10.1146/annurev-physchem-032210-103424. PMID: 21219151
7. Digman MA, Gratton E (2009) Imaging barriers to diffusion by pair correlation functions. Biophys J 97: 665-673. doi: 10.1016/j.bpj.2009.04.048. PMID: 19619481
8. Földes-Papp Z (2006) What it means to measure a single molecule in a solution by fluorescence fluctuation spectroscopy. Exp Mol Pathol 80: 209-218. doi: 10.1016/j.yexmp.2006.01.001. PMID: 16515783
9. Földes-Papp Z (2007) Fluorescence fluctuation spectroscopic approaches to the study of a single molecule diffusing in solution and a live cell without systemic drift or convection: a theoretical study. Curr Pharm Biotechnol 8: 261-273. doi: 10.2174/138920107782109930. PMID: 17979724
10. Földes-Papp Z (2013) Measurements of single molecules in solution and live cells over longer observation times than those currently possible: the meaningful time. Curr Pharm Biotechnol 14: 441-444. doi: 10.2174/1389201011314040009. PMID: 23369193
11. Földes-Papp Z, Baumann G, Kinjo M, Tamura M (2004) Single-phase single-molecule fluorescence correlation spectroscopy (SPSM-FCS). In: Fuchs J, Podda M, editors. Encyclopedia of medical genomics and proteomics. New York: Taylor & Francis, pp. 1-7.
12. Baumann G, Place RF, Földes-Papp Z (2010) Meaningful interpretation of subdiffusive measurements in living cells (crowded environment) by fluorescence fluctuation microscopy. Curr Pharm Biotechnol 11: 527-543. doi: 10.2174/138920110791591454. PMID: 20553227
13. Földes-Papp Z (2015) Individual macromolecule motion in a crowded living cell. Curr Pharm Biotechn 16: 1-2. doi: 10.2174/1389201016666141229103953. PMID: 25543662
14. Saxton MJ (2006) A biological interpretation of transient anomalous subdiffusion. I. Qualitative model. Biophys J 92: 1178-1191. doi: 10.1529/biophysj.106.092619. PMID: 17142285
15. Odde DJ, Buettner HM (1998) Autocorrelation function and power spectrum of two-state random processes used in neurite guidance. Biophys J 75: 1189-1196. doi: 10.1016/S0006-3495(98)74038-X. PMID: 9726921
16. Meroz Y, Sokolov IM, Klafter J.(2010) Subdiffusion of mixed origins: when ergodicity and nonergodicity coexist. Phys Rev E Stat Nonlin Soft Matter Phys 81: 010101. doi: 10.1103/PhysRevE.81.010101. PMID: 20365308
17. Baumann G, Gryczynski I, Földes-Papp Z (2010) Anomalous behavior in length distributions of 3D random Brownian walks and measured photon count rates within observation volumes of single-molecule trajectories in fluorescence fluctuation microscopy. Opt Express 18: 17883-17896. doi: 10.1364/OE.18.017883. PMID: 20721175
18. Li L, Okino ST, Zhao H, Pookot D, Place RF, et al. (2006) Small dsRNAs induce transcriptional activation in human cells. Proc Natl Acad Sci USA 103: 17337-17342. doi: 10.1073/pnas.0607015103. PMID: 17085592
19. Guo D, Barry L, Lin SSH, Huang V, Li L (2014) RNAa in action: from the exception to the norm. RNA Biol 11: 1221-1225. doi: 10.4161/15476286.2014.972853. PMID: 25602906
20. Portnoy V, Lin SHS, Li KH, Burlingame A, Hu Z, et al. (2016) saRNA-guided Ago2 targets the RITA complex to promoters to stimulate transcription. Cell Res 26: 320-335. doi: 10.1038/cr.2016.22. PMID: 26902284
21. Kang MR, Li G, Pan T, Xing J, Li L (2017) Development of Therapeutic dsP21-322 for Cancer Treatment. Adv Exp Med Biol 983: 217-229. doi: 10.1007/978-981-10-4310-9_16. PMID: 28639203
22. Place RF, Noonan EJ, Földes-Papp Z, Li L (2010) Defining features and exploring chemical modifications to manipulate RNAa activity. Curr Pharm Biotechnol 11: 518-526. doi: 10.2174/138920110791591463. PMID: 20662764
23. Földes-Papp Z , König K , Studier H, Bückle R, Breunig HG, Uchugonova A, Kostner GM (2009) Trafficking of mature miRNA-122 into the nucleus of live liver cells. Curr Pharm Biotechn 10: 569-578. doi: 10.2174/138920109789069332. PMID: 19619125
24. Földes-Papp Z, Costa JM, Demel U, Tilz GP, Kinjo M, et al. (2004) Specifically associated PCR products probed by coincident detection of two-color cross-correlated fluorescence intensities in human gene polymorphisms of methylene tetrahydrofolate reductase at site C677T: a novel measurement approach without follow-up mathematical analysis. Exp Mol Pathol 76: 212-218. doi: 10.1016/j.yexmp.2003.12.007. PMID: 15126103
25. Földes-Papp Z, Kinjo M, Tamura M, Birch-Hirschfeld E, Demel U, et al. (2005) A new ultrasensitive way to circumvent PCR-based allele distinction: direct probing of unamplified genomic DNA by solution-phase hybridization using two-color fluorescence cross-correlation spectroscopy. Exp Mol Pathol 78: 177-189. doi: 10.1016/j.yexmp.2005.01.005. PMID: 15924869
26. Földes-Papp Z, Liao SJ, You T, Terpetschnig E, Barbieri B (2010) Confocal fluctuation spectroscopy and imaging. Curr Pharm Biotechnol 11: 639-653. doi: 10.2174/138920110792246618. PMID: 20497113
27. Gielen E, Smisdom N, vandeVen M, De Clercq B, Gratton E, et al. (2009) Measuring diffusion of lipid-like probes in artificial and natural membranes by raster image correlation spectroscopy (RICS): use of a commercial laser-scanning microscope with analog detection. Langmuir 25: 5209-5218. doi: 10.1021/la8040538. PMID: 19260653
28. Földes-Papp Z, Liao SJ, Barbieri B, Gryczynski JrK, Luchowski R, et al. (2011) Single actomyosin motor interactions in skeletal muscle. Biochim Biophys Acta 1813: 858-866. doi: 10.1016/j.bbamcr.2011.02.001. PMID: 21315775
29. Yadav R, Lu HP (2018) Probing Dynamic heterogeneity in aggregated ion channels in live cells. J Phys Chem C 122: 13716-13723. doi: 10.1021/acs.jpcc.8b00262.s001. PMID: 10
30. Yan H, Li B, Wang J (2019) Non-equilibrium landscape and flux reveal how the central amygdala circuit gates passive and active defensive responses. J R Soc Interface 16: 20180756. doi: 10.1098/rsif.2018.0756. PMID: 30966954
31. Vezzani A, Barkai E, Burioni R (2019) Single-big-jump principle in physical modeling. Phys Rev E 100: 12108. doi: 10.1103/PhysRevE.100.012108. PMID: 31499929
32. Baumann G, Kinjo M, Földes-Papp Z (2014) Anomalous subdiffusive measurements by fluorescence correlations spectroscopy and simulations of translational diffusive behavior in live cells. J Biol Methods 1: e3. doi: 10.14440/jbm.2014.17.